Smart Materials and Structures

PAPER

Active damping of multiferroic composite plates using 1–3 piezoelectric composites

To cite this article: S C Kattimani 2017 *Smart Mater. Struct.* **26** 125021

View the article online for updates and enhancements.

Related content

- Smart damping of geometrically nonlinear vibrations of laminated composite beams usingvertically reinforced 1–3 piezoelectric composites
S K Sarangi and M C Ray
- Active constrained layer damping of geometrically nonlinear vibrations of functionallygraded plates using piezoelectric fiber-reinforced composites
Satyajit Panda and M C Ray
- Theoretical and experimental investigations on the active structural–acoustic control of athin plate using a vertically reinforced 1-3 piezoelectric composite
M C Ray, A Faye, S Patra et al.

Recent citations

- Orthogonal Anisotropic Sensing and Actuating Characteristics of a 1-3 PZT Piezoelectric Microfiber Composite
Andong Wang *et al*
- Semi-analytical analysis of static and dynamic responses for laminated magneto-electro-elastic plates
Pengchong Zhang *et al*
- Effective properties and nonlinearities in 1-3 piezocomposites: a comprehensive review
R Pramanik and A Arockiarajan

This content was downloaded from IP address 14.139.155.214 on 24/09/2020 at 06:42

IOP Publishing Smart Materials and Structures
Smart Mater. Struct. **26** (2017) 125021 (15pp) https://doi.org/10.1088/1361-665X/aa96d5

Active damping of multiferroic composite plates using 1–3 piezoelectric composites

S C Kattimani

Department of Mechanical Engineering, National Institute of Technology Karnataka-Surathkal-575025, India

E-mail: sck@nitk.ac.in

Received 8 November 2016, revised 23 October 2017
Accepted for publication 30 October 2017
Published 10 November 2017

Abstract

A layer-wise shear deformation theory is used to analyze the smart damping of multiferroic composite or magneto-electro-elastic (MEE) plates. The intent of this analysis is to investigate the need for incorporating additional smart elements for controlling the vibrations of multiferroic composite plates. Active constrained layer damping (ACLD) treatment has been incorporated to alleviate the vibration of MEE plate. A layer of viscoelastic material is used as constrained layer for the ACLD treatment. The coupled constitutive equations of multiferroic (ferroelectric and ferromagnetic) composite materials along with the total potential energy principle are used to derive the finite element formulation for the overall multiferroic or MEE plate. Maxwell's electrostatic and electromagnetic relations are used to compute the electric and magnetic potential distribution. Influence of obliquely reinforced piezoelectric fibers in the piezoelectric layer of the ACLD treatment has also been investigated. In order to investigate the importance of using ACLD treatment for an active damping of multiferroic or MEE plate, an active control of MEE plate has also been analyzed by providing the control voltage directly to the piezoelectric layers of the MEE substrate plate without using the ACLD treatment. The present study suggests that for an optimal control of MEE plates, the smartness element such as the ACLD treatment is essentially required.

Keywords: multiferroic composite, magneto-electro-elastic, active control, active constrained layer damping

(Some figures may appear in colour only in the online journal)

1. Introduction

Advanced technologies coupled with advanced manufacturing of composites have permitted the integration of smart composites not only in the aeronautical industries but also in the fields of automotive, civil, marine and medical industries. It is evident from the literature that the piezoelectric ceramic materials exhibit dominant role in the field of active vibration control of featherweight adaptable structures because of the advantages offered by these materials like; they are hard, dense and can be manufactured to almost any shape or size. Consequently, piezoelectric transducers have become increasingly popular in vibration control applications due their piezoelectric and converse effects. They can be used as sensors and as actuators in structural vibration control systems. In addition, they provide excellent actuation and sensing capabilities on account of their ability to transform mechanical energy into electrical energy and vice versa. Bailey and Hubbard [1] designed an active vibration damper for cantilever beam using distributed-parameter actuator made of piezoelectric polymer (vinylidene fluoride). Crawley *et al* [2] developed an analytical and experimental piezoelectric actuators as elements of intelligent structures. Baz and Poh [3] utilized the piezoelectric actuators to control the vibrations flexible beams while Clark *et al* [4] used the piezoelectric actuators for thin plates. Reddy [5] presented a theoretical formulation and finite element model of the laminated composite plate integrated with piezoelectric sensors and actuators. Using a piezoelectric material, active constrained layer damping (ACLD) of plates is studied by Baz and Ro [6] and this concept is used to control the vibration of structures [7–10]. The piezoelectric effect of the piezo-ceramic materials assured as a promising candidate for sensors and actuators in flexible structures. The sensors and actuators made of

 © 2017 IOP Publishing Ltd Printed in the UK

piezo-ceramic materials combined with the flexible structures, accomplish the cause of control and monitor the health of structural system. Such structures amalgamated with the piezoelectric layer/patches with self-regulating and guiding capabilities are generally termed as 'smart structures'. If the distributed actuators are made of monolithic piezoelectric materials having small coupling constants, high control voltage is required to alleviate the vibrations of flexible host structures. Hence, the research on the development of ACLD treatment using low-control-coefficient solid piezoelectric materials is evolved [11]. The typical ACLD treatment consists of a viscoelastic layer (constrained layer) which is sandwiched between the piezoelectric layer (constraining layer) and the substrate (host structure). If the piezoelectric layer of the ACLD treatment is not activated with applied voltages, the ACLD treatment turns into passive constrained layer damping (PCLD) treatment due to the presence of viscoelastic layer in the middle of substrate structure and piezoelectric layer. Thus, the ACLD treatment has gained more importance and established as an efficient control system because of providing both active and passive damping effect at the same time during the operation of the structure [12, 13]. For over a decade, Ray and his coworkers [14–19] have been carrying out the extensive research on using the ACLD treatment for active control of composite plates and shells. They have observed that the considerable enhancement of the damping characteristics of laminated composite structures when the piezoelectric fiber orientation angle is zero in the constraining layer of the ACLD treatment. Chantalakhana and Stanway [20] used the ACLD treatment for a composite plate with clamped-clamped boundary conditions. Optimization of an active and passive damping of the hybrid active-passive laminated sandwich plate with viscoelastic core was studied by Araújo *et al* [21]. The same work has been extended by Araújo *et al* [22] for a sandwich plate with piezoelectric sensor and actuator bonded on the exterior faces. An optimal positioning of piezoelectric patch location for has also been studied.

Recently, an interesting and unique class of composites known as multiferroic or magneto-electro-elastic (MEE) composite consisting of ferroelectric/piezoelectric ($BaTiO_3$) and ferromagnetic/piezomagnetic ($CoFe_2O_4$) phases has attracted the interest of researchers on account of promising properties of multiferroic materials. Composite structures made of piezoelectric and magnetostrictive layers are subjected not only to the geometrical and material property constraints but also to the coupled actions of electro-elastic, magneto-elastic, and electro-magnetic fields which are absent in the individual constituents. A distinguished feature of the multiferroic composite materials is that they possess the capability of transforming the energies among elastic, electric and magnetic fields forming electro-elastic, magneto-elastic and electro-magnetic coupling effects [23, 24]. These interesting properties might have led the researchers to use multiferroic composite materials in the field of control system, micro-electro-mechanical systems, precision instruments and medical instruments like ultrasonic imaging devices etc. Hence, it is necessary to take care and caution while designing new smart structures consisting of multiferroic composites. Many researchers have paid their attention to the problems related to MEE structures. Pan and Heyliger put together a great effort to study the free vibration analysis [23] and static fields [24] of MEE multilayered rectangular plates under simply supported edge conditions with different electrical boundary conditions. They noticed the similarity with pure piezoelectric plates for some of the lower order natural frequencies. Liu and Chang [25] obtained the closed form expression for the transverse vibration of MEE plate and demonstrated the natural frequencies of two-layered $BaTiO_3$ (barium titanate)—$CoFe_2O_4$ (cobalt ferrite) plate for different volume fractions of $BaTiO_3$. Ramirez *et al* [26] analyzed the free vibration of functionally graded MEE plates using a discrete layer model and obtained the natural frequencies for different aspect ratios, gradation type, and boundary conditions. Buchanan [27] obtained the natural frequencies of MEE infinite plate and compared with those of multiphase composite plate. Lage *et al* [28] studied the static analysis of MEE plate using layerwise partial mixed finite element model. Pan [29] used a propagator matrix method to derive an exact solution for three-dimensional multi-layered MEE plates and later extended to FG MEE plates by Pan and Han [30]. Wang *et al* [31] implemented the state vector approach to analyze multilayered MEE plate. The same approach is used for free vibration of MEE hybrid laminated plates by Wang *et al* [32]. Moita *et al* [33] used the higher order shear deformation theory to develop a finite element model for the static and free vibration analysis of MEE plates. Chen *et al* [34] derived the independent state equations for the free vibration analysis of isotropic MEE plates and they noticed that the coupling coefficients have no effect on lower order natural frequencies. Bhangale and Ganesan used the finite element method to investigate on free vibration of FG MEE plates [35] and cylindrical shell [36]. They also noticed that the effects of MEE coupling terms are insensitive to some of the lower modes. Chen *et al* [37] studied the free vibration of FG multilayered MEE plates.

Most recently, Gou *et al* [38] investigated the static deformation of anisotropic four layered MEE plates under surface loading based on the modified couple-stress theory. Xin and Hu [39] analyzed the free vibration of simply supported multilayered MEE plates by using the state space approach and the discrete singular convolution algorithm. Reddy's third-order shear deformation theory was implemented to study the free vibration of a MEE rectangular plate by Shooshtari and Razavi [40]. Further, nonlinear analysis of MEE plates has been attracted the considerable interest of researchers. Shooshtari and Razavi [41] investigated a nonlinear free and forced vibration of transversely isotropic rectangular MEE thin plate using thin plate theory along with the von Kármán procedure. They extended the same procedure for linear and nonlinear free vibration of multilayered MEE doubly curved shell on elastic foundation [42] and also studied the nonlinear free vibration of symmetric MEE laminated rectangular plate using first order shear deformation theory (FSDT) [43]. Kattimani and Ray [44, 45] investigated on the control of geometrically nonlinear vibrations of MEE plates and shells using 1–3 piezoelectric composites (PZC) then later extended their study for FG MEE plates [46]. In

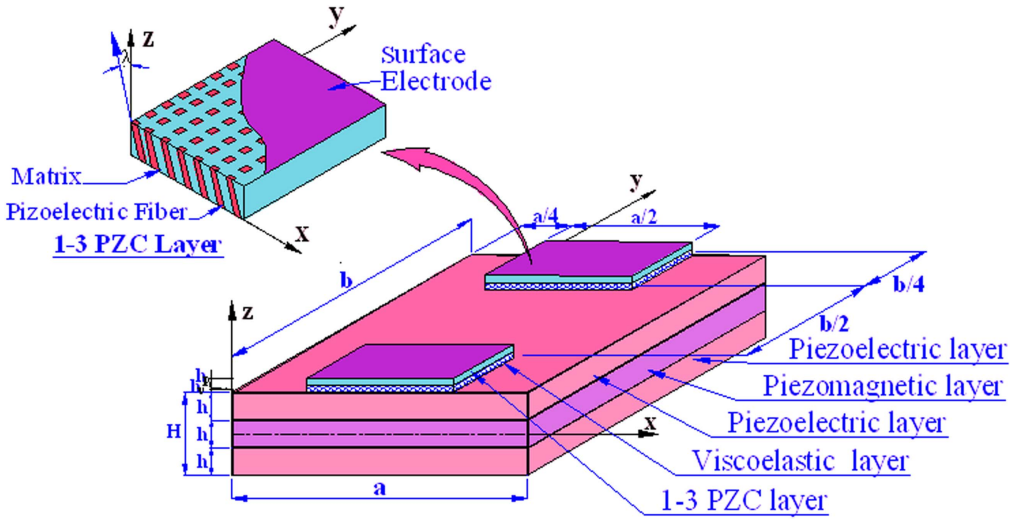

Figure 1. Schematic diagram of a B/F/B multiferroic or magneto-electro-elastic plate integrated with two patches of ACLD treatment composed of 1–3 PZC constraining layer.

addition, the comprehensive research on MEE plates and shells has been investigated as a doctoral study by Kattimani [47]. Milazzo [48] presented a smart laminate free vibration of FG MEE plate using refined equivalent single layer models. He has also studied the influence of large deflections on MEE plate response using FSDT [49]. Farajpour *et al* [50] investigated the nonlinear free vibration of size dependent MEE nanoplates subjected to external electric and magnetic potentials by considering the geometrical nonlinearity.

Since, the multiferroic or MEE plate composed of smart materials can be a promising smart composite structure for various applications, the necessity of using the additional means of smart damping such as ACLD treatment for active control of multiferroic plates must be investigated. However, to the author's best knowledge, the research concerning to the control of multiferroic plates is not yet been reported in the literature. In this paper, the author contemplates analyzing the performance of ACLD treatment for active damping of multiferroic composite plates. For the aforesaid investigation, a finite element formulation has been derived to analyze the active damping multiferroic plate integrated with the patches of the ACLD treatment. The influence of different parameters such as the effect of coupling coefficients, boundary conditions, aspect ratio and the orientation of piezoelectric fiber in the piezoelectric constraining layer of the ACLD treatment on the response of the MEE plates have been thoroughly investigated. The viscoelastic layer is used as the constrained layer of the ACLD treatment. The frequency dependence of the viscoelastic material has also been studied. The necessity of the ACLD treatment is examined by inactivating the ACLD patches and providing the feedback control system directly to the piezoelectric layers of the MEE sandwich plate.

2. Problem description and governing equations

A multiferroic composite plate with the ACLD treatment consisting of two patches placed on the top surface of the top layer of the substrate plate is schematically represented in figure 1. The middle layer of the composite plate is made of ferromagnetic (magnetostrictive) while the bottom and the top layers of the plate are made of ferroelectric (piezoelectric). The viscoelastic layer is sandwiched between the piezoelectric layer of the ACLD treatment and the MEE substrate plate. The expanded view of figure 1 demonstrates the orientation of the piezoelectric fiber reinforcement in the 1–3 PZC layer. The fiber orientation angle with z-axis is represented by λ and the fibers are coplanar with xz-plane. However, for the same orientation angle (λ), the piezoelectric fibers can be considered as coplanar with yz-plane also. The length a, width b and the total thickness H are considered along with the x-, y-, and z-directions, respectively, while h_p and h_v are the thickness of the constraining PZC layer and the constrained viscoelastic layer of the ACLD treatment, respectively. The equivalent single layer displacement theory cannot be used to describe the structure made of layers of dissimilar materials, for the reason that distinct in orders of the elastic properties in the adjacent continua of the overall structure. Consequently, the kinematics of the deformation of the overall structure is defined by the layerwise shear deformation theory [44]. The coupled constitutive relations for the multiferroic composite solid substrate are given by

$$\{\sigma_b^s\} = [\bar{C}_b^s]\{\varepsilon_b^s\} - \{e_b^s\}E_z - \{q_b^s\}H_z \text{ and}$$
$$\{\sigma_s^s\} = [\bar{C}_s^s]\{\varepsilon_s^s\}, \quad (1)$$

$$D_z = \{e_b^s\}^T\{\varepsilon_b^s\} + \in_{33}^s E_z + d_{33}H_z, \quad (2)$$

$$B_z = \{q_b^s\}^T\{\varepsilon_b^s\} + d_{33}E_z + \mu_{33}H_z, \quad (3)$$

where, D_z, E_z, B_z, and H_z are the electric displacement, electrical field, magnetic induction, magnetic field, respectively, along the z-direction; $[\overline{C}_b^s]$ and $[\overline{C}_s^s]$ are transformed elastic coefficient matrices; μ_{33} and $\in_{33}^s$ are the magnetic permeability constant and dielectric constant, respectively; d_{33}, $\{e_b^s\}$ and $\{q_b^s\}$ the electromagnetic coefficient, piezoelectric coefficient vector and the magnetostrictive coefficient vector, respectively. Further, the superscript s refers to the substrate,

subscript b refers to bending, s refers to shear and T indicates matrix transpose.

The conventional complex modulus approach is employed to model the viscoelastic layer. The viscoelastic material used in the present study is assumed to be linearly viscoelastic homogeneous and isotropic. The Young's modulus E and the shear modulus G of the viscoelastic material in the complex modulus approach are given by

$$E = 2G(1 + \upsilon) \text{ and } G = G'(1 + \mathrm{i}\eta) \tag{4}$$

in which ν is the Poisson ratio, G' is the storage modulus and η is the loss factor at any particular operating temperature and frequency. Thus, the constitutive relation for the viscoelastic layer corresponding to the transverse shear stresses and strains is given by

$$\{\sigma_s^v\} = [\overline{C}_s^v]\{\varepsilon_s^v\} \tag{5}$$

in which $[\overline{C}_s^v] = \begin{bmatrix} 1 & 0 \\ 0 & 1 \end{bmatrix}$, where, the superscript v represents the viscoelastic layer. In the present method of finite element formulation, the compatible constitutive relations for the 1–3 PZC constraining piezoelectric layer of the ACLD treatment are given by

$$\begin{aligned} \{\sigma_b^p\} &= [\bar{C}_b^p]\{\varepsilon_b^p\} - [\bar{C}_{bs}]\{\varepsilon_s^p\} - \{e_b^p\}E_z \text{ and} \\ \{\sigma_s^p\} &= [\bar{C}_{bs}]^T\{\varepsilon_b^p\} + [\bar{C}_s^p]\{\varepsilon_s^p\} - \{e_s^p\}E_z \end{aligned} \tag{6}$$

In equation (6), superscript p refers to piezoelectric layer, while the transformed elastic coefficient matrices and coupling elastic constant matrix $[\overline{C}_{bs}]$ are given by

$$[\overline{C}_b^p] = [\overline{C}_b^s] \text{ and } [\overline{C}_s^p] = [\overline{C}_s^s].$$

However, the coupling elastic matrices when the orientation of the piezoelectric fibers coplanar with the vertical xz- or yz-plane, respectively are given by

$$[\overline{C}_{bs}] = \begin{bmatrix} \overline{C}_{15} & 0 \\ \overline{C}_{25} & 0 \\ \overline{C}_{35} & 0 \\ 0 & \overline{C}_{46} \end{bmatrix} \text{ or } [\overline{C}_{bs}] = \begin{bmatrix} 0 & \overline{C}_{14} \\ 0 & \overline{C}_{24} \\ \overline{C}_{56} & 0 \\ 0 & \overline{C}_{34} \end{bmatrix}. \tag{7}$$

If the piezoelectric fibers are coplanar with both the xz- and the yz-planes, the coupling matrix turns into a null matrix. In addition, the piezoelectric coefficient matrices $\{e_b^p\}$ and $\{e_s^p\}$ appearing in equation (6), contain the transformed effective piezoelectric coefficients of the 1–3 PZC as follows:

$$\begin{aligned} \{e_b^p\} &= \{\overline{e}_{31} \;\; \overline{e}_{32} \;\; \overline{e}_{33} \;\; \overline{e}_{36}\}^T \text{ and} \\ \{e_s^p\} &= \{\overline{e}_{35} \;\; \overline{e}_{34}\}^T. \end{aligned} \tag{8}$$

The first variations of the potential energies of the substrate δT_{ps}, the viscoelastic layer δT_{pv} and the piezoelectric actuator layer δT_{pp} for the B/F/B plate can be expressed as follows:

$$\begin{aligned} \delta T_{ps} = &\int_{\Omega} \delta\{\varepsilon_b^s\}^T\{\sigma_b^s\}\mathrm{d}\Omega + \int_{\Omega} \delta\{\varepsilon_s^s\}^T\{\sigma_s^s\}\mathrm{d}\Omega \\ &- \int_A Q_1^{\phi}\delta\bar{\phi}_1\mathrm{d}A - \int_A Q^{\psi}\delta\bar{\psi}\mathrm{d}A \\ &- \int_A Q_2^{\phi}\delta\bar{\phi}_2\mathrm{d}A - \int_{\Omega^t} \delta E_z^t D_z^t \mathrm{d}\Omega^t \\ &- \int_{\Omega^b} \delta E_z^b D_z^b \mathrm{d}\Omega^b - \int_{\Omega^m} \delta H_z B_z \mathrm{d}\Omega^m \\ &- \int_A P\delta w\mathrm{d}A, \end{aligned} \tag{9}$$

$$\delta T_{pv} = \int_{\Omega} \delta\{\varepsilon_s^v\}^T\{\sigma_s^v\}\mathrm{d}\Omega^e, \tag{10}$$

$$\begin{aligned} \delta T_{pp} = &\int_{\Omega^e} \delta\{\varepsilon_b^p\}^T\{\sigma_b^p\}\mathrm{d}\Omega^e \\ &+ \int_{\Omega^e} \delta\{\varepsilon_s^p\}^T\{\sigma_s^p\}\mathrm{d}\Omega - \int_{\Omega^e} E_z D_z \mathrm{d}\Omega, \end{aligned} \tag{11}$$

where Q_1^{ϕ} is the surface electric charge density of the top piezoelectric layer, Q_2^{ϕ} is the surface electric charge density of the bottom piezoelectric layer, Q^{ψ} is the surface magnetic charge density of the middle magnetostrictive layer and P is the applied transverse distributed load on the top surface of the top piezoelectric layer of the MEE plate. Since the thickness of the viscoelastic layer considered is very small compared to the thickness of other layers and its axial elastic constants are much lower than that of the other layers, the strain energy of this layer corresponding to the normal strains is negligible and is not considered here. According to Maxwell's electromagnetic equations, the transverse electric field E_z and the magnetic field H_z are related to the electric potential ϕ and the magnetic potential ψ in the following forms,

$$E_z = -\frac{\partial\phi}{\partial z} \text{ and } H_z = -\frac{\partial\psi}{\partial z} \tag{12}$$

It should be noted that for very small layer thickness, the variation of the electric potential and the magnetic potential functions may be assumed linear. Also, the interfaces between the piezoelectric layer and the magnetostrictive layer are duly grounded. Consequently, the electric potential functions for the top piezoelectric layer (ϕ^t), the bottom piezoelectric layer (ϕ^b) and the magnetic potential distribution field in the middle magnetostrictive layer (ψ) of the composite substrate can be expressed respectively as follows:

$$\phi^t = \frac{z - z_1}{h}\bar{\phi}_1,\ \phi^b = -\frac{z - h_2}{h}\bar{\phi}_2 \text{ and } \psi = \frac{z - h_2}{h}\bar{\psi}, \tag{13}$$

where, z_1 and h_2 are the bottom surface of the top piezoelectric layer and the top surface of the bottom piezoelectric layer of the substrate along the z-coordinate, respectively; $\overline{\phi}_1$ and $\overline{\phi}_2$ are electric potentials on the top and the bottom surface of the piezoelectric layer while $\overline{\psi}$ is the magnetic potential on the top surface of the magnetostrictive layer. The thickness of each layer of the substrate is h. It should also be noted that equations (9)–(13) can be augmented for the F/B/F stacking

sequence of the MEE plate by reinstating the top and the bottom ferroelectric layers with the ferromagnetic layers, while the middle layer is ferroelectric.

3. Finite element formulation

The overall substrate plate integrated with the ACLD patches is discretized by eight noded iso-parametric quadrilateral elements. The size of the mesh for computing the numerical results is considered as 4 × 4. This results in the total number of translational degrees of freedom as 195 while the total number of rotational degrees of freedom is 520. The generalized displacement vectors $\{d_{ti}\}$ and $\{d_{ri}\}$ associated with the ith ($i = 1, 2, 3, \ldots, 8$) node of the quadrilateral element can be written as

$$\begin{aligned}\{d_{ti}\} &= [u_{0i} \quad v_{0i} \quad w_{0i}]^T \text{ and}\\ \{d_{ri}\} &= [\theta_{xi} \quad \theta_{yi} \quad \theta_{zi} \quad \phi_{xi} \quad \phi_{yi} \quad \phi_{zi} \quad \gamma_{xi} \quad \gamma_{yi}]^T,\end{aligned} \tag{14}$$

where, the subscript t and r represent the translational and rotational, respectively. The nodal generalized displacement vectors ($\{d_t^e\}$ and $\{d_r^e\}$), the nodal electric potential vector $\{\phi^e\}$ and the nodal magnetic potential vector $\{\overline{\psi}^e\}$ at any point within the element can be written as

$$\begin{aligned}&\{d_t\} = [N_t]\{d_t^e\},\ \{d_r\} = [N_r]\{d_r^e\},\\ &\{\phi\} = \left[\overline{\phi}_1 \quad \overline{\phi}_2\right]^T = [N_\phi]\{\phi^e\} \text{ and}\\ &\overline{\psi} \quad = [N_\psi]\{\overline{\psi}^e\}.\end{aligned} \tag{15}$$

The various terms appearing in equation (15) are explicitly presented in appendix A. Using equations (12)–(15), the transverse electric fields E_z^t, E_z^b and the transverse magnetic field H_z can be expressed as

$$\begin{aligned}E_z^t &= -\frac{1}{h}[1 \quad 0][N_\phi]\{\phi^e\},\\ E_z^b &= -\frac{1}{h}[0 \quad 1][N_\phi]\{\phi^e\} \text{ and}\\ H_z &= -\frac{1}{h}[N_\psi]\{\overline{\psi}^e\}.\end{aligned} \tag{16}$$

Now, using the kinematic strain-displacement relations [44] and equation (13), the strain vectors at any point within the element can be obtained in terms of the nodal generalized displacement vectors [44]. Substituting the nodal generalized displacement vectors into equations (9)–(11), and recognizing that $Q_1^\phi = \varepsilon_{33}\frac{V_1}{h}$ and $Q_2^\phi = \varepsilon_{33}\frac{V_2}{h}$ with V_1 and V_2 being the applied voltages across the thickness of the top and the bottom ferroelectric layers of the substrate plate, the first variation of the total potential energy of the typical element combined with the ACLD treatment can be written as follows:

$$\begin{aligned}\delta T_p^e = {} & \delta\{d_t^e\}^T[K_{tt}^e]\{d_t^e\} + \delta\{d_t^e\}^T[K_{tr}^e]\\ & \times \{d_r^e\} + \delta\{d_r^e\}^T[K_{tr}^e]^T\{d_t^e\}\\ & + \delta\{d_r^e\}^T[K_{rr}^e]\{d_r^e\} + \delta\{d_t^e\}^T[K_{t\phi}^e]\\ & \times \{\overline{\phi}^e\} + \delta\{d_r^e\}^T[K_{r\phi}^e]\{\phi^e\} + \delta\{d_t^e\}^T\\ & \times [K_{t\psi}^e]\{\overline{\psi}^e\} + \delta\{d_r^e\}^T[K_{r\psi}^e]\{\overline{\psi}^e\}\\ & + \delta\{\phi^e\}^T([K_{t\phi}^e]^T\{d_t^e\} + [K_{r\phi}^e]^T\\ & \times \{d_r^e\} - [K_{\phi\phi}^e]^T\{\phi^e\}) - \delta\{d_t^e\}\{F_t^e\}\\ & + \delta\{\overline{\psi}^e\}^T([K_{t\psi}^e]^T\{d_t^e\} + [K_{r\psi}^e]^T\\ & \times \{d_r^e\} - [K_{\psi\psi}^e]\{\overline{\psi}^e\}) - \delta\{\phi^e\}^T\\ & \times \{F_{1\phi}^e\}V_1 - \delta\{\phi^e\}^T\{F_{2\phi}^e\}V_2\\ & - \delta\{\overline{\psi}^e\}^T\{F_\psi^e\} - \delta\{d_t^e\}^T\{F_t^e\}\\ & + \delta\{d_t^e\}^T\{F_{rp}^e\}V + \delta\{d_r^e\}^T\{F_{tp}^e\}V.\end{aligned} \tag{17}$$

The first variation of the kinetic energy of the element can be written as

$$\delta T_k^e = -\delta\{d_t^e\}^T[M^e]\{\ddot{d}_t^e\}. \tag{18}$$

In equations (17) and (18), $[M^e]$ is the elemental mass matrix; $[K_{tt}^e]$, $[K_{tr}^e]$ and $[K_{rr}^e]$ are the elemental elastic stiffness matrices; $[K_{t\phi}^e]$, $[K_{r\phi}^e]$ and $[K_{t\psi}^e]$, $[K_{r\psi}^e]$ are the elemental electro-elastic and the elemental magneto-elastic coupling stiffness matrices, respectively; $[K_{\phi\phi}^e]$ and $[K_{\psi\psi}^e]$ are the elemental electrical and magnetic stiffness matrices, respectively; $\{F_{tp}^e\}$, $\{F_{rp}^e\}$, $\{F_t^e\}$, $\{F_\phi^e\}$ and $\{F_\psi^e\}$ are the elemental electro-elastic coupling load vectors, mechanical load vector, electrical load vector and the elemental magnetic load vector, respectively. The applied voltage across the thickness of the 1–3 PZC layer is represented by V. It may be noted that the substrate considered here is very thin. Therefore, the rotary inertia has been ignored for the estimation of the kinetic energy of the element. Applying Hamilton's variational principle given by

$$\int_{t_1}^{t_2} \delta(T_p^e - T_k^e)\mathrm{d}t = 0 \tag{19}$$

The elemental equations of motion for the overall plate are derived and assembled to obtain the coupled global equations of motion as follows:

$$\begin{aligned}&[M]\{\ddot{X}\} + [K_{tt}]\{X\} + [K_{tr}]\{X_r\} + [K_{t\phi}]\{\phi\}\\ &\quad + [K_{t\psi}]\{\psi\} = \{F\} - \sum_{j=1}^{q}\{F_{tp}^j\}V^j\\ &[K_{tr}]^T\{X\} + [K_{rr}]\{X_r\} + [K_{r\phi}]\{\phi\}\\ &\quad + [K_{r\psi}]\{\psi\} = -\sum_{j=1}^{q}\{F_{rp}^j\}V^j\\ &[K_{t\phi}]^T\{X\} + [K_{r\phi}]^T\{X_r\} - [K_{\phi\phi}]\{\phi\} = \{F_\phi\}\\ &[K_{t\psi}]^T\{X\} + [K_{r\psi}]^T\{X_r\} - [K_{\psi\psi}]\{\psi\} = \{F_\psi\}.\end{aligned} \tag{20}$$

The global electro-elastic coupling vectors $\{F_{tp}^j\}$ and $\{F_{rp}^j\}$ in equation (20) becomes null vectors for the elements without integrated with the ACLD treatment and the stiffness matrices

will be real. The mass matrix $[M]$ and various stiffness matrices $[K_{ii}]$ appearing in equation (20) without superscript e represent the global mass matrix and global stiffness matrices, respectively. $\{F\}$, ($\{F_\phi\} = \{F_{1\phi}\}V_1 + \{F_{2\phi}\}V_2$) and $\{F_\psi\}$ are the global nodal mechanical load vector, the global nodal electrical load vector and the global nodal magnetic load vector, respectively, $\{X\}$, $\{X_r\}$, $\{\phi\}$ and $\{\psi\}$ are the global generalized nodal displacement vectors, electrical potential, and magnetic potential vectors, respectively. The number of ACLD patches is q and V^j is the applied voltage to the jth ACLD patch. It is interesting to know that the coupled global equations derived above also govern the passive (uncontrolled) constrained layer damping (PCLD) in the absence of the applied control voltage. Further, the global stiffness matrices for an element attached to the ACLD treatment will be complex and hence the energy dissipation characteristics of the overall MEE plate are attributed to the imaginary part of these matrices.

4. Closed loop model

A simple derivative control law has been utilized to supply the control voltage V^j for the constraining piezoelectric layer of each ACLD patch. Thus, the supply control voltage for each patch can be written in the form of derivatives of the global nodal degrees of freedom as follows:

$$V^j = -K_d^j \dot{w}_o = -K_d^j [U_t^j]\{\dot{X}\}. \tag{21}$$

Similarly, the control voltages for the top and the bottom piezoelectric layers of the substrate plate can be written as follows:

$$\begin{aligned} V_1 &= -K_{d1}\dot{w}_o = -K_{d1}[U_1]\{\dot{X}\} \text{ and} \\ V_2 &= -K_{d2}\dot{w}_o = -K_{d2}[U_2]\{\dot{X}\}, \end{aligned} \tag{22}$$

where, K_{d1} and K_{d2} are the control gains of the jth ACLD patch, the top piezoelectric layer and the bottom piezoelectric layer of the MEE plate, respectively. $[U_t^j]$, $[U_1]$ and $[U_2]$ are the unit vectors at a particular point to express the transverse velocity in terms of the time derivative of the global nodal generalized translational displacements. On substitution of equations (21) and (22) into equation (20), the final coupled governing equations of motion for the closed loop dynamics of the multiferroic MEE plate integrated with the ACLD patches can be expressed as follows:

$$\begin{aligned} &[M]\{\ddot{X}\} + [K_{tt}]\{X\} + [K_{tr}]\{X_r\} + [K_{t\phi}]\{\phi\} \\ &\quad + [K_{t\psi}]\{\psi\} + \sum_{j=1}^{q}\{F_{tp}^j\}K_d^j[U_t^j]\{\dot{X}\} = \{F\} \\ &[K_{tr}]^T\{X\} + [K_{rr}]\{X_r\} + [K_{r\phi}]\{\phi\} \\ &\quad + [K_{r\psi}]\{\psi\} + \sum_{j=1}^{q}\{F_{rp}^j\}K_d^j[U_t^j]\{\dot{X}\} = 0 \\ &[K_{t\phi}]^T\{X\} + [K_{r\phi}]^T\{X_r\} - [K_{\phi\phi}]\{\phi\} + \{F_{1\phi}\} \\ &\quad \times K_{d1}[U_1]\{\dot{X}\} + \{F_{2\phi}\}K_{d2}[U_2]\{\dot{X}\} = 0 \\ &[K_{t\psi}]^T\{X\} + [K_{r\psi}]^T\{X_r\} - [K_{\psi\psi}]\{\psi\} = \{F_\psi\}. \end{aligned} \tag{23}$$

The global nodal rotational degrees of freedom, the global nodal electric potential degrees of freedom and the global nodal magnetic potential degrees of freedom can be condensed to obtain the global equations of motion in terms of the global translational degrees of freedom only as follows:

$$\begin{aligned} &[M]\{\ddot{X}\} + \left(\sum_{j=1}^{q}\{F_p^j\}K_d^j[U^j] + [K_{a\phi}]\{F_{1\phi}\}\right. \\ &\quad \left.\times K_{d1}[U_1] + [K_{a\phi}]\{F_{2\phi}\}K_{d2}[U_2]\right)\{\dot{X}\} \\ &\quad + [K]\{X\} = \{F\}, \end{aligned} \tag{24}$$

where the global augmented matrices are as follows:

$$\begin{aligned} [K] &= [K_1] - [K_2][K_3]^{-1}[K_2]^T, \\ \{F_p^j\} &= [K_2]\,[K_3]^{-1}\{F_{rp}^j\} - \{F_{tp}^j\}, \\ [K_{a\phi}] &= [K_{t\phi}]\,[K_{\phi\phi}]^{-1} \\ &\quad - [K_2]\,[K_3]^{-1}[K_{r\phi}][K_{\phi\phi}]^{-1}, \\ [K_{a\psi}] &= [K_{t\psi}]\,[K_{\psi\psi}]^{-1} \\ &\quad - [K_2]\,[K_3]^{-1}[K_{r\psi}][K_{\psi\psi}]^{-1}, \\ [K_1] &= [K_{tt}] + [K_{t\phi}][K_{\phi\phi}]^{-1}[K_{t\phi}]^T \\ &\quad + [K_{t\psi}][K_{\psi\psi}]^{-1}[K_{t\psi}]^T, \\ [K_2] &= [K_{tr}] + [K_{t\phi}][K_{\phi\phi}]^{-1}[K_{r\phi}]^T \\ &\quad + [K_{t\psi}][K_{\psi\psi}]^{-1}[K_{r\psi}]^T, \\ [K_3] &= [K_{rr}] + [K_{r\phi}][K_{\phi\phi}]^{-1}[K_{r\phi}]^T \\ &\quad + [K_{r\psi}][K_{\psi\psi}]^{-1}[K_{r\psi}]^T, \end{aligned} \tag{25}$$

Assuming that the overall plate undergoes harmonic motion, the solution of $\{X\}$ and the load vector $\{F\}$ can be considered as

$$\{X\} = \{\overline{X}\}e^{i\omega t} \text{ and } \{F\} = \{\overline{F}\}e^{i\omega t} \tag{26}$$

in which $\{\overline{X}\}$ and $\{\overline{F}\}$ are the amplitudes of the displacements and the forcing function, respectively and ω is the frequency of excitation. Using equation (26), equation (25) can be expressed in the impedance form for computing the frequency response functions as follows:

$$\{\overline{X}\} = [K_{\text{eq}}]\{\overline{F}\} \tag{27}$$

in which

$$\begin{aligned} [K_{\text{eq}}] = -\omega^2[M] + i\omega&\left(\sum_{j=1}^{q}\{F_p^j\}K_d^j[U^j]\right. \\ &+ [K_{a\phi}]\{F_{1\phi}\}K_{d1}[U_1] + [K_{a\phi}] \\ &\left.\times\{F_{2\phi}\}K_{d2}[U_2]\right) + [K] \end{aligned} \tag{28}$$

Further, in order to study the frequency dependence of viscoelastic material, the Golla–Hughes–McTavish (GHM) model has been considered in the present analysis. The material modulus function $s\tilde{G}(s)$ in the present study is expressed by a single mini-oscillator term [52] as follows:

$$s\tilde{G}(s) = G^\infty\left[1 + \alpha\frac{s^2 + 2\hat{\xi}\hat{\omega}s}{s^2 + 2\hat{\xi}\hat{\omega}s + \hat{\omega}^2}\right] \tag{29}$$

in which, G^∞ is the equilibrium value of the modulus i.e. the final value of the relaxation $G(t)$. Each mini-oscillator term consisting of three positive constants α, $\hat{\omega}$ and $\hat{\xi}$. These constants influence the shape of the modulus function in the

Table 1. Material properties of $BaTiO_3$ and $CoFe_2O_4$ [29].

	$C^{11} = C^{22}$ (10^9 N m^{-2})	C^{12} (10^9 N m^{-2})	$C^{13} = C^{23}$ (10^9 N m^{-2})	C_{33} (10^9 N m^{-2})	$C^{44} = C^{55}$ (10^9 N m^{-2})	C^{66} (10^9 N m^{-2})	ρ (kg m^{-3})
$BaTiO_3$	166	77	78	162	43	44.5	5800
$CoFe_2O_4$	286	173	170.5	269.5	45.3	56.5	5300
$BaTiO_3$	$e^{31} = e^{32}$ (C m^{-2})−4.4	e^{33} (C/m^2) 18.6	$e^{24} = e^{15}$ (C m^{-2}) 11.6	$\in_{11} = \in_{22}$ (10^{-9} C^2 N^{-1} m^{-2}) 11.2	$\in_{33}$ (10^{-9} C2 N^{-1} m^{-2}) 12.6	$\mu_{11} = \mu_{22}$ (10^{-6} N s^{-2} C^{-2}) 5	μ_{33} (10^{-6} N s^2 C^{-2}) 10
$CoFe_2O_4$	$q_{31} = q_{32}$ (N Am^{-1}) 180.3	q_{33} (N Am^{-1}) 699.7	$q_{24} = q_{15}$ (N Am^{-1}) 550	$\in_{11} = \in_{22}$ (10^{-9} C^2 N^{-1} m^{-2}) 0.08	$\in_{33}$ (10^{-9} C^2 N^{-1} m^{-2}) 0.093	$\mu_{11} = \mu_{22}$ (10^{-6} N s^{-2} C^{-2})−590	μ_{33} (10^{-6} N s^2 C^{-2}) 157

complex s-domain. Further, introducing the auxiliary dissipation coordinates Z and Z_r as follows:

$$s\tilde{G}(s)\{\tilde{X}_t\} = G^{\infty}[(1+\alpha)\{\tilde{X}_t\} - \alpha\tilde{Z}(s)] \text{ and}$$
$$s\tilde{G}(s)\{\tilde{X}_r\} = G^{\infty}[(1+\alpha)\{\tilde{X}_r\} - \alpha\tilde{Z}_r(s)], \quad (30)$$

$$\tilde{Z}(s) = \frac{\hat{\omega}^2}{s^2 + 2\hat{\xi}\hat{\omega}s + \hat{\omega}^2}\{X_t\} \text{ and}$$
$$\tilde{Z}_r(s) = \frac{\hat{\omega}^2}{s^2 + 2\hat{\xi}\hat{\omega}s + \hat{\omega}^2}\{X_r\}. \quad (31)$$

Making use of the Laplace transformations, and simplifying equations (27)–(31) to obtain the global equation of motion as follows:

$$[M^*]\{\ddot{X}\} + [C^*]\{\dot{X}\} + [K^*]\{X\} = \{F^*\} + \sum_{j=1}^{q}\{\overline{F}_p^j\}V^j, \quad (32)$$

where,

$$[M^*] = \begin{bmatrix}[M] & 0 & 0\\ 0 & I_Z & 0\\ 0 & 0 & I_{Z_r}\end{bmatrix}, [C^*] = \begin{bmatrix}0 & 0 & 0\\ 0 & 2\xi\hat{\omega} & 0\\ 0 & 0 & 2\xi\hat{\omega}\end{bmatrix},$$
$$[K^*] = \begin{bmatrix}[K_x] & [K_z] & [K_{zr}]\\ -\hat{\omega}^2 & \hat{\omega}^2 & 0\\ \hat{\omega}^2[K_5] & -\hat{\omega}^2[K_6] & \hat{\omega}^2[K_7]\end{bmatrix},$$
$$\{F^*\} = \begin{Bmatrix}\{F\}\\ 0\\ 0\end{Bmatrix}, \{\overline{F}_p^j\} = \begin{Bmatrix}\{F_p^j\}\\ 0\\ \{F_{pz}^j\}\end{Bmatrix}, \{X\} = \begin{Bmatrix}\{X_t\}\\ Z\\ Z_r\end{Bmatrix}. \quad (33)$$

5. Results and discussions

The finite element formulation derived in the earlier section is used to compute the frequency responses of the multiferroic composite (MEE) plates attached with the ACLD treatment. Two ACLD patches are placed on the top surface of the top layer of the substrate plate as illustrated in figure 1. The numerical results are estimated for the MEE plate by activating/deactivating the ACLD patches by means of supply control voltage. The sizes of the patches are selected according to the size of the substrate plate as the width and the length of the patches are 25% and 50% of the width and length the of the substrate plate, respectively. The material of the piezoelectric layer of the ACLD patches is spur epoxy/PZT-5H composite with 60% piezoelectric fiber volume fraction. The properties of this constraining piezoelectric layer are considered from literature [20]. The thicknesses of the viscoelastic layer and the constraining 1–3 PZC layer are considered to be 50.8 μm and 250 μm, respectively. The material properties of the piezoelectric and magnetostrictive layers of the MEE plates are listed in table 1. Unless otherwise mentioned, the square plate of length a and width b are taken as 0.5 m while thickness H is considered as 0.003 m with three layers of equal thickness

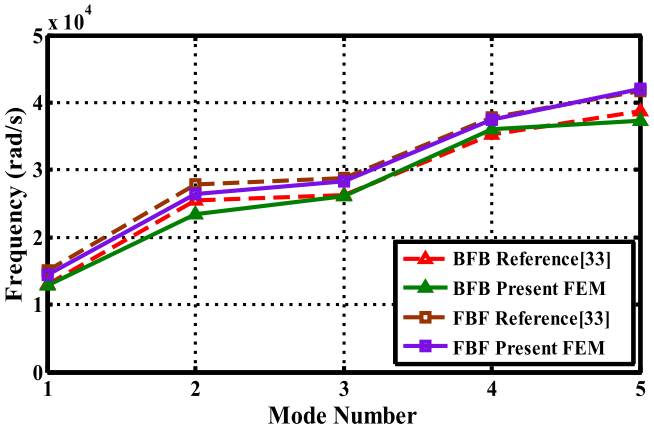

Figure 2. Comparison of natural frequencies of simply supported MEE plate integrated with inactive ACLD patches of negligible thickness with those of identical MEE plate [33].

$h = 0.001$ m. The generally used stacking sequence B/F/B and F/B/F are considered in the present analysis. The values of the complex shear modulus, the Poisson's ratio and the density of the constrained viscoelastic layer are used as $20(1+i)$ MNm^{-2}, 0.49 and 1140 Kg m^{-3}, respectively [20]. The boundary conditions for the MEE plates employed are as follows:

For simply supported

At $x = 0$ and a; $v_0 = w_0 = \theta_y = \phi_y = \gamma_y = \theta_z = \phi_z = 0$

At $y = 0$ and b; $u_0 = w_0 = \theta_x = \phi_x = \gamma_x = \theta_z = \phi_z = 0$.

For clamped-clamped

At $x = 0$ and a; $y = 0$ and b; $u_0 = v_0 = w_0 = \theta_x = \theta_y = \phi_x = \phi_y = \gamma_y = \theta_z = \phi_z = 0$

In all cases the electric and magnetic potentials at the boundaries are assumed to be zero. A time-harmonic point force of magnitude 1 N is applied at the point $(a/2, b/4, H/2)$ to excite the first few modes of the MEE plate. The open-loop and the closed-loop responses of the MEE plate have been examined by the frequency response functions for the transverse displacement at the point $(a/2, b/4, H/2)$. The control voltages supplied to the patch 1 and the patch 2 are negatively proportional to the velocities of the points $(a/2, b/4, H/2)$ and $(a/2, 3b/4, H/2)$, respectively. Within the acceptable control voltage, the arbitrary value of control gains are selected for the acceptable control of first few vibrating modes of the MEE plate. Unless otherwise stated, the controlled responses are computed for the piezoelectric fiber orientation $\lambda = 0°$ in the 1–3 PZC (Vertically reinforced 1–3 PZC). The FE formulation derived here can be used for studying the purely elastic/piezoelectric/piezomagnetic laminated composite plate by changing the layers of the MEE plate with the conventional composite/piezoelectric/piezomagnetic layers. Consequently, to facilitate validation of the present FE formulation, the fundamental natural frequencies of homogeneous purely elastic laminated composite plates with the inactive ACLD patches of trivial thickness are calculated and compared with analytical results available in the literature for

Table 2. Comparison of fundamental natural frequency parameter $\bar{\omega} = \omega(a^2/H)\sqrt{\rho/E_T}$, ω is the circular frequency.

Source	$a/H = 10$	$a/H = 100$
Present FE soln.	12.498	15.217
Reddy [51]	12.223	15.185

the same laminated composite plates [50]. Table 2 demonstrates this comparison of fundamental natural frequency parameters for different aspect ratios. It may be observed that the two sets of results are in very good agreement. A further validation is carried out with the existing solutions available in the literature [33] for the identical MEE plates with inactivated ACLD patches of negligible thickness. A square plate of sides $a = b = 1$ m and the thickness $H = 0.3$ m studied by Moita *et al* [33] is considered here for this validation. Figure 2 illustrates this comparison of some of the lowest natural frequencies of MEE plates for the B/F/B and the F/B/F stacking sequences while table 3 demonstrates the same in numerical values. It may be observed from this figure that the present results are in very good agreement with those reported in [33] for both the stacking sequences of the MEE plates. However, as expected, it has been noticed that the fundamental natural frequencies obtained by the present analysis are slightly lower than the fundamental frequencies obtained in [33]. This is attributed to the consideration of transverse normal strain ε_z in the present model which is neglected in [33].

It is now imperative to examine if the MEE plate can be controlled without using the ACLD patches. Hence, first, the MEE plate with B/F/B stacking sequence has been analyzed with inactivated ACLD patches of negligible thickness by providing the control voltage directly across the thickness of the top and the bottom ferroelectric layers whereas, for the plate with F/B/F stacking sequence, the control voltage is applied across the middle ferroelectric layer. For the B/F/B plate, the control voltages supplied to the ferroelectric layers are negatively proportional to the velocities of the points ($a/2$, $b/4$, $H/2$) and ($a/2$, $b/4$, $-H/2$) of the top and the bottom ferroelectric layers, respectively. In case of the F/B/F stacking sequence, the velocity of the point ($a/2$, $b/4$, $h/2$) is fed back for applying the control voltage across the middle ferroelectric layer. The arbitrary values of control gains have been selected for controlling the first few modes of vibrations of the MEE plates. Figures 3 and 4 illustrate the uncontrolled ($K_d = K_{d1} = K_{d2} = 0$) and controlled frequency response functions of simply supported and clamped-clamped B/F/B plates, respectively, with inactive ($K_d = 0$) ACLD patches of negligible thickness. Further, it is also noticed that the second mode of vibration cannot be controlled by activating the top ($K_{d1} = 300$, $K_{d2} = K_d = 0$) or the bottom ($K_{d2} = 300$, $K_{d1} = K_d = 0$) piezoelectric layer of the B/F/B MEE plate. It is also noticed that if both the piezoelectric layers are simultaneously activated, the substrate is not controlled as shown in figure 5. In case of the F/B/F configuration, figure 6 illustrates that the active middle piezoelectric layer cannot control the MEE plate. Figures 7 and 8 illustrate the frequency response functions for the simply supported plates when the constraining layer of the ACLD patches are passive (PCLD) and active while figures 9 and 10 demonstrate the same for the clamped-clamped multiferroic composite plates. It can be observed from these figures that the active

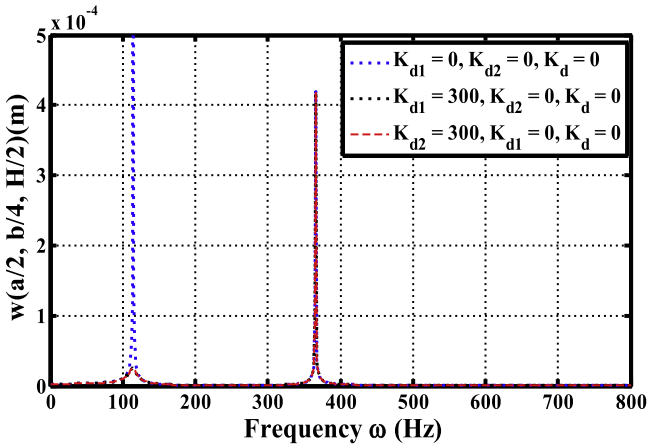

Figure 3. Frequency response functions for the transverse displacement $w(a/2, b/4, H/2)$ of a simply supported B/F/B MEE plate integrated with inactive ACLD patches of negligible thickness.

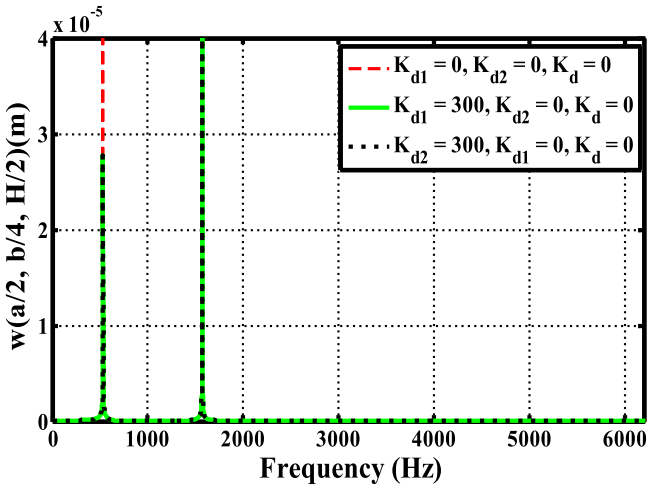

Figure 4. Frequency response functions for the transverse displacement $w(a/2, b/4, H/2)$ of a clamped-clamped B/F/B MEE plate integrated with inactive ACLD patches of negligible thickness.

Table 3. Comparison of natural frequencies (rad s^{-1}) of MEE plate obtained in the present analysis with the result of Moita *et al* [33].

	B/F/B		F/B/F	
Mode	Present	Reference [33]	Present	Reference [33]
1	12977.23	13024.78	14390.51	15043.32
2	24477.05	25401.26	26420.411	27880.80
3	26337.85	26256.34	28257.37	28795.37
4	34723.05	35206.62	37477.55	37753.16
5	38880.38	38671.99	41980.56	41649.71
6	38880.38	38671.99	41980.56	41649.71

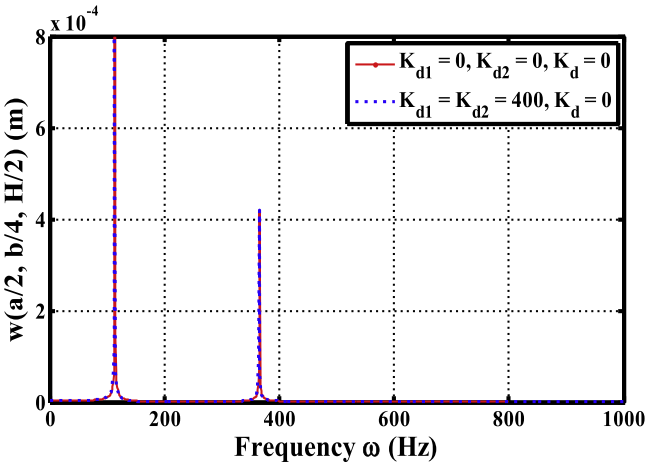

Figure 5. Frequency response functions for the transverse displacement $w(a/2, b/4, H/2)$ of a simply supported B/F/B MEE plate integrated with inactive ACLD patches of negligible thickness.

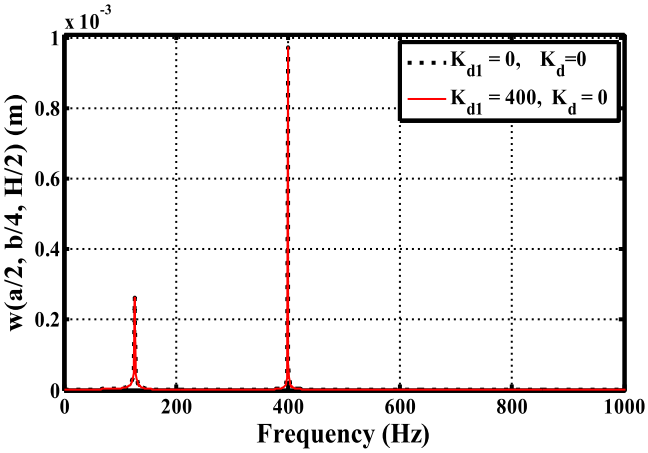

Figure 6. Frequency response functions for the transverse displacement $w(a/2, b/4, H/2)$ of a simply supported F/B/F MEE plate integrated with inactive ACLD patches of negligible thickness.

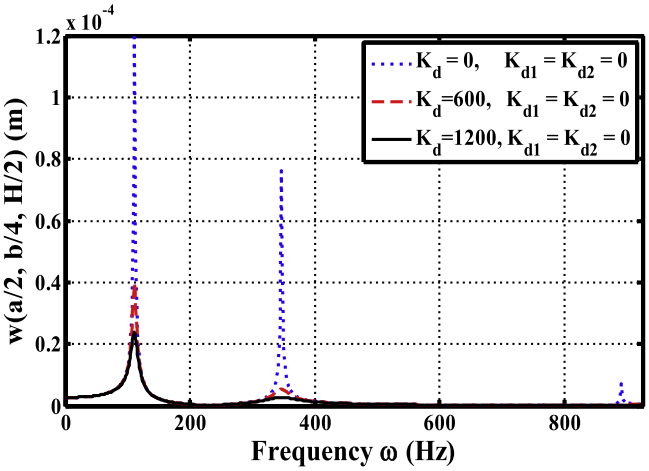

Figure 7. Frequency response functions for the transverse displacement $w(a/2, b/4, H/2)$ of a simply supported B/F/B MEE plate using activated ACLD patches.

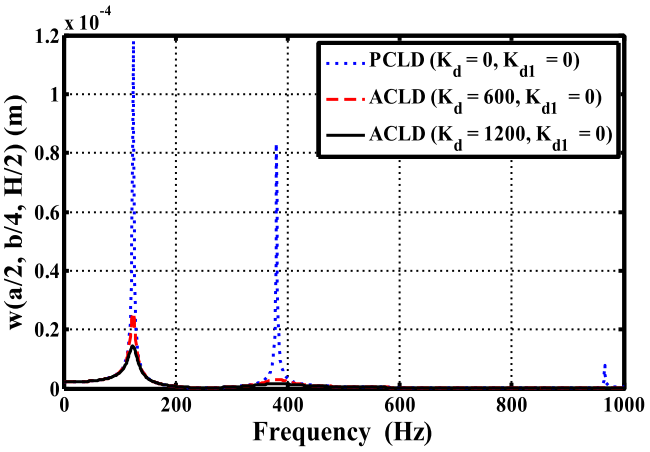

Figure 8. Frequency response functions for the transverse displacement $w(a/2, b/4, H/2)$ of a simply supported F/B/F MEE plate using activated ACLD patches.

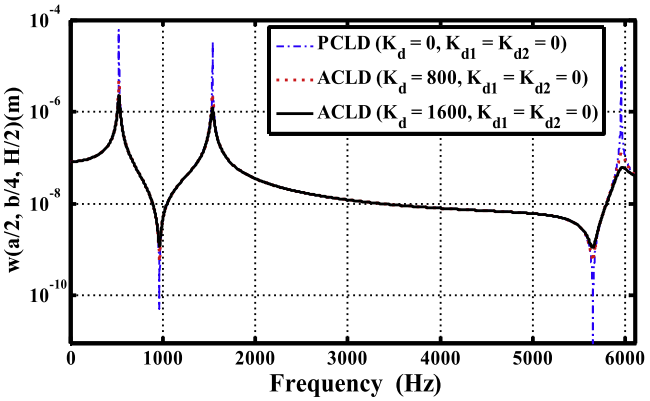

Figure 9. Frequency response functions for the transverse displacement $w(a/2, b/4, H/2)$ of a clamped-clamped B/F/B MEE plate using activated ACLD patches.

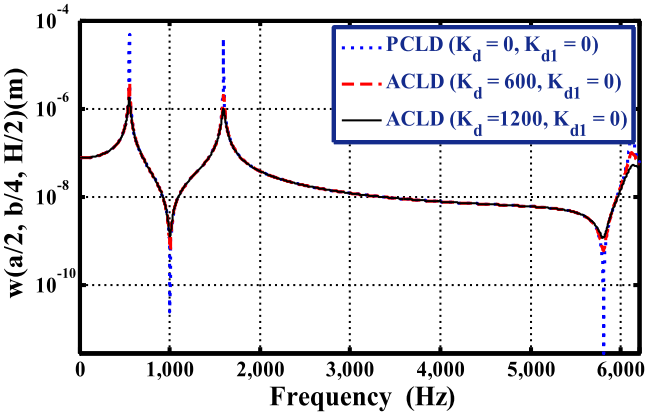

Figure 10. Frequency response functions for the transverse displacement $w(a/2, b/4, H/2)$ of a clamped-clamped F/B/F MEE plate using activated ACLD patches.

constraining layer of the vertically reinforced 1–3 PZC layer ($\lambda = 0°$) significantly improves the damping characteristics of the multiferroic plates and the active ACLD patches control all the modes considered. With the intention that the other researchers may verify their models, hence the first three

Table 4. Frequency parameters of magneto-electro-elastic plate ($H = 0.003$ m).

SS-1	B/F/B			F/B/F		
Mode	$a/H = 10$	$a/H = 50$	$a/H = 100$	$a/H = 10$	$a/H = 50$	$a/H = 100$
1	0.379	0.079	0.040	0.426	0.090	0.046
2	0.896	0.207	0.114	0.998	0.236	0.128
3	0.938	0.217	0.119	1.042	0.246	0.134
C–C						
1	0.683	0.195	0.139	0.771	0.216	0.149
2	1.309	0.489	0.387	1.444	0.533	0.408
3	1.355	0.497	0.392	1.495	0.542	0.414

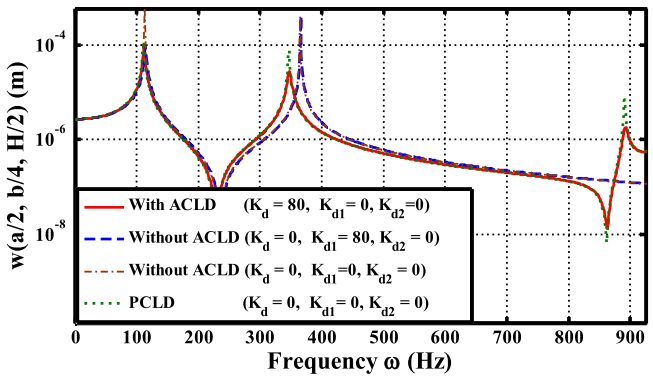

Figure 11. Comparison of active damping of the simply supported B/F/B MEE plate without the use of the ACLD patches with that of the same using ACLD patches.

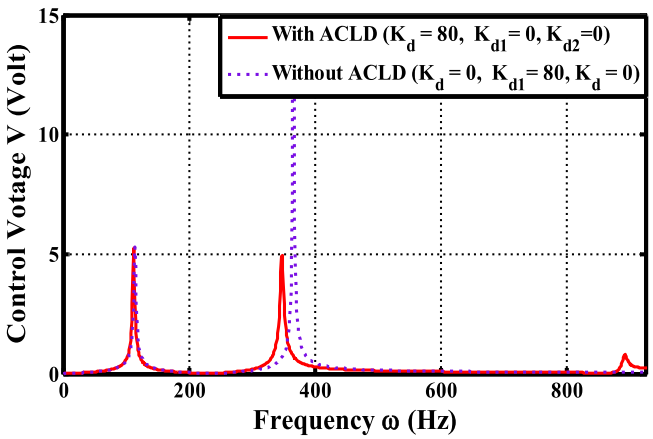

Figure 12. Comparison of the control voltage for active damping of the simply supported B/F/B MEE plate without the use of the ACLD patches with that of the same using ACLD patches.

frequency parameters $\omega^* = \omega a\sqrt{\rho_{\max}/C_{\max}}$ ($C_{\max}$ being the maximum of the C_{ij} in the whole sandwich plate [23]) of the simply supported as well as clamped-clamped MEE plates of different aspect ratios ($a/H = 10$, 50 and 100) are presented in table 4. Figures 11 and 12 illustrate the comparison of frequency response functions for the transverse displacement and the control voltage, respectively, for the active damping of a simply supported B/F/B MEE plate with ($K_d \neq 0$, $K_{d1} = K_{d2} = 0$) and without ($K_d = 0$, $K_{d1} \neq 0$ or $K_{d2} \neq 0$) activating the ACLD patches. It may be observed from these figures that the control voltage and the transverse displacement are almost equal in both the cases corresponding to the first mode while the second mode has not been controlled, if the piezoelectric layers of the plate are directly activated ($K_d = 0$, $K_{d1} \neq 0$ or $K_{d2} \neq 0$). Figures 13 and 14 illustrate the same for the clamped-clamped MEE plate. It can be noticed from these figures that considerably high voltage is

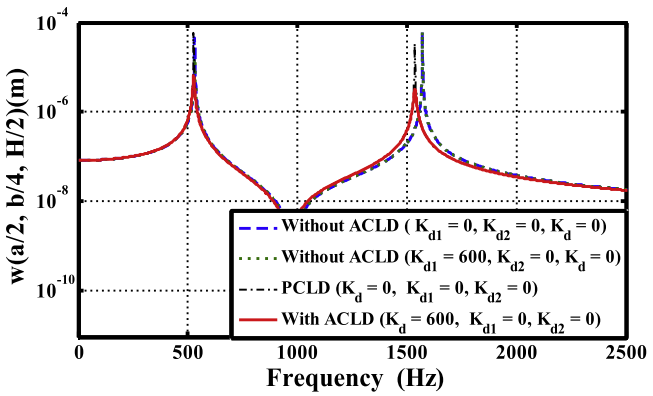

Figure 13. Comparison of active damping of the clamped-clamped B/F/B MEE plate without using the ACLD patches with that of the same using ACLD patches.

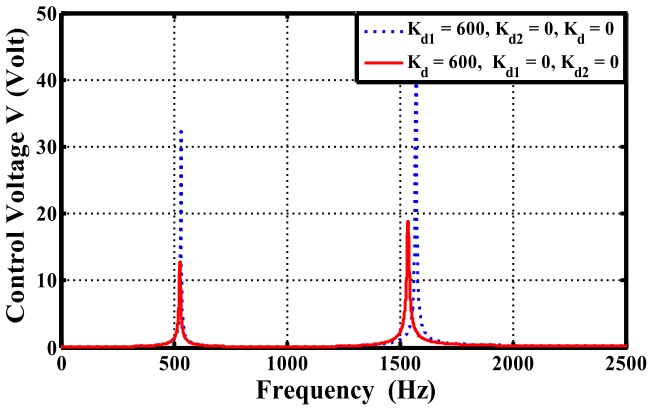

Figure 14. Comparison of the control voltage for active damping of the clamped-clamped B/F/B MEE plate without the use of the ACLD patches with that of the same using ACLD patches.

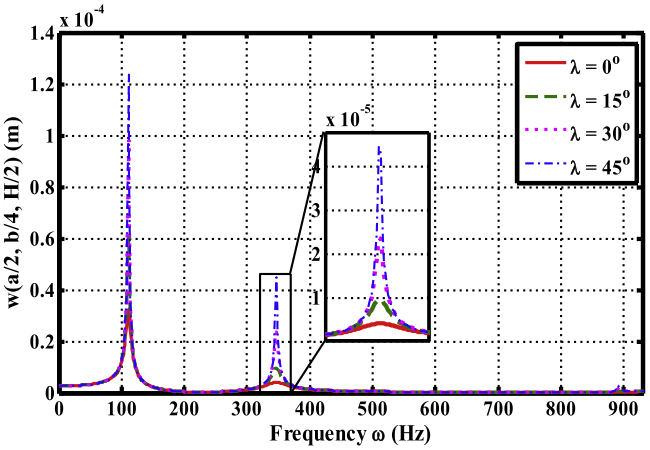

Figure 15. Effect of variation of piezoelectric fiber orientation angle (λ) in xz-plane on the controlled response of a simply supported B/F/B MEE plate ($K_d = 800$).

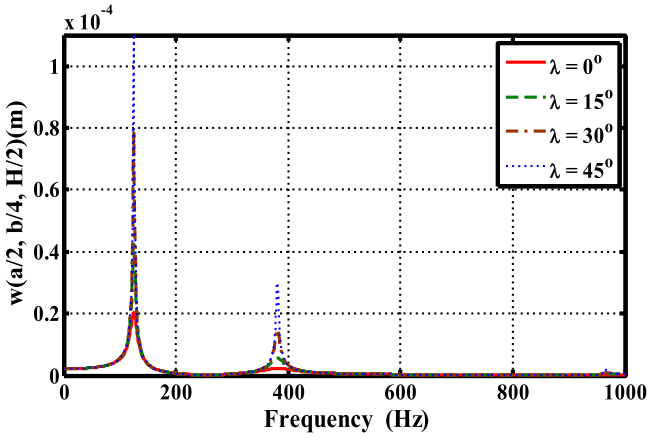

Figure 17. Effect of variation of piezoelectric fiber orientation angle (λ) in xz-plane on the controlled response of a simply supported F/B/F MEE plate ($K_d = 800$).

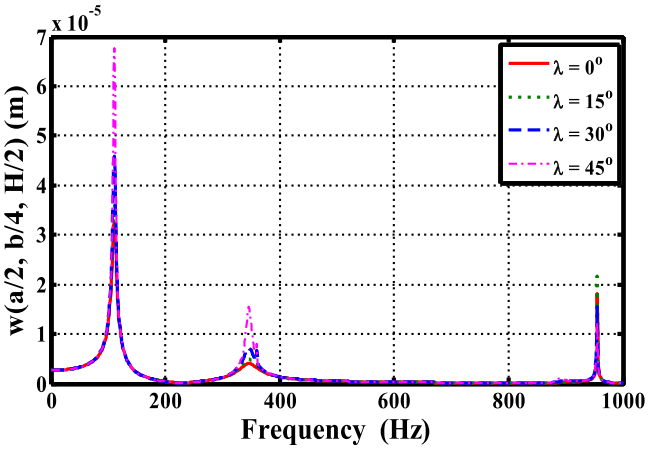

Figure 16. Effect of variation of piezoelectric fiber orientation angle (λ) in yz-plane on the controlled response of a simply supported B/F/B MEE plate ($K_d = 800$).

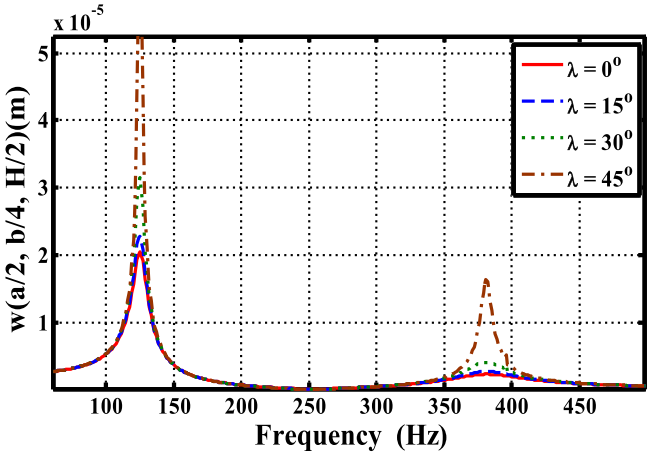

Figure 18. Effect of variation of piezoelectric fiber orientation angle (λ) in yz-plane on the controlled response of a simply supported F/B/F MEE plate ($K_d = 800$).

required to control the first mode of vibration of the MEE plate, if the piezoelectric layers of the plate are directly activated ($K_d = 0$, $K_{d1} \neq 0$ or $K_{d2} \neq 0$) as compared to the control voltage required using the active ACLD patches ($K_d \neq 0$, $K_{d1} = K_{d2} = 0$). Thus, for the optimum control of MEE plates, ACLD patches are essentially required to control first few important modes of vibrations of MEE plates with the usage of very low control voltage. Figures 15–18 illustrate the effect of variation of the fiber orientation angle (λ) in the piezoelectric layer of the ACLD patches on the frequency response functions of simply supported smart MEE plates ($a = b = 0.5$ m, $K_d = 800$). The numerical values of controlled amplitudes of clamped-clamped MEE plate are tabulated in table 5 for better interpretation. It may be noticed that the best control of these plates is achieved by the vertically reinforced 1–3 PZC layer ($\lambda = 0°$). It may also be observed from these figures that the performance of obliquely reinforced 1–3 PZC constraining layer in which the piezoelectric fibers are coplanar with the yz-plane is better than that of the obliquely reinforced 1–3 PZC constraining layer wherein, the piezoelectric fibers are coplanar with the xz-plane.

The effects of ferro-elastic or electro-elastic and the magneto-elastic couplings may be excluded by setting the stiffness matrices $[K_{t\phi}]$, $[K_{\phi\phi}]$, $[K_{t\psi}]$ and $[K_{\psi\psi}]$ to null matrices. As a result, the responses of the multiferroic composite plate will be free from these coupling effects. Figures 19 and 20 illustrate the influence of the ferro-elastic and the magneto-elastic coupling on the controlled, coupled, and uncoupled responses of a simply supported B/F/B plates when the ACLD patches are inactive ($K_d = 0$, $K_{d1} \neq 0$ or $K_{d2} \neq 0$) and active ($K_d \neq 0$, $K_{d1} = K_{d2} = 0$), respectively. Table 6 demonstrates these results in numerical values for the first two natural frequencies. It be observed from these figures and from the table 6 that the ferro-elastic and magneto-elastic couplings cause a marginal increase in stiffening of the multiferroic plate. Further, higher attenuation of the fundamental mode of vibration is noticed when the MEE plate is controlled by the ACLD patches. In addition, the frequency

Table 5. Effect of piezoelectric fiber orientation angle (λ) on the controlled natural frequencies of clamped-clamped MEE plate.

Piezoelectric fiber orientation angle (λ)		Mode	Frequencies	0° w (m)	15° w (m)	30° w (m)	45° w (m)
B/F/B	xz-plane	1	527	4.76E-06	6.75E-06	1.60E-05	3.14E-05
		2	1536	2.42E-06	3.65E-06	1.20E-05	8.24E-06
		3	5957	1.20E-07	1.43E-07	1.84E-07	2.54E-07
	yz-plane	1	527	4.76E-06	6.75E-06	1.32E-05	2.06E-05
		2	1536	2.42E-06	3.65E-06	8.24E-06	7.57E-06
		3	5957	1.20E-07	1.43E-07	1.86E-07	5.31E-07
F/B/F	xz-plane	1	552	2.74E-06	6.55E-06	1.40E-05	9.08E-05
		2	1597	1.44E-06	3.30E-06	7.19E-06	2.72E-05
		3	6129	7.59E-08	1.88E-07	3.20E-07	1.19E-06
	yz-plane	1	552	2.74E-06	3.51E-06	6.11E-06	4.69E-05
		2	1597	1.44E-06	1.92E-06	3.58E-06	9.68E-06
		3	6129	7.59E-08	8.83E-08	1.23E-07	3.45E-07

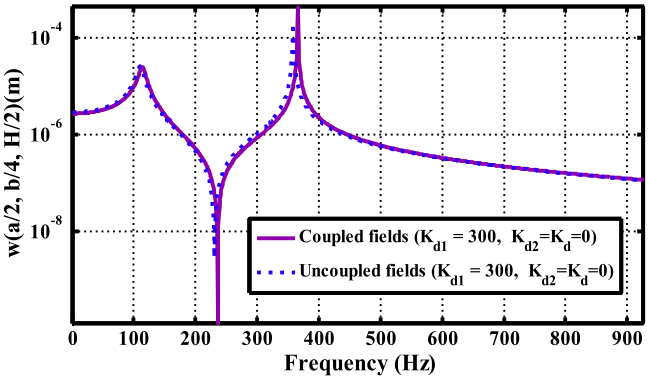

Figure 19. Effects of electro-elastic and magneto-elastic couplings on the frequency response of simply supported B/F/B MEE plate with inactive ACLD patches of negligible thickness.

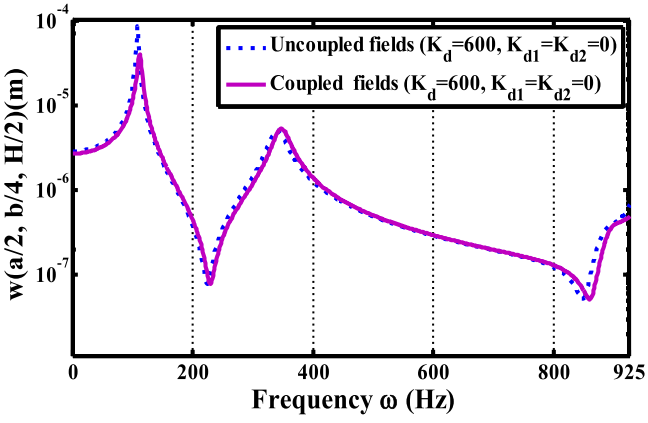

Figure 20. Effects of electro-elastic and magneto-elastic couplings on the frequency response of simply supported B/F/B MEE plate controlled by activated ACLD patches.

dependence of viscoelastic material has also been studied briefly by using GHM method. In a single term GHM expression, the values of the constants α, $\hat{\xi}$ and $\hat{\omega}$ are used as 11.42, 20 and 1.0261 × 105, respectively [53]. The shear modulus (G^{∞}) and the density of the viscoelastic material (ρ_v)

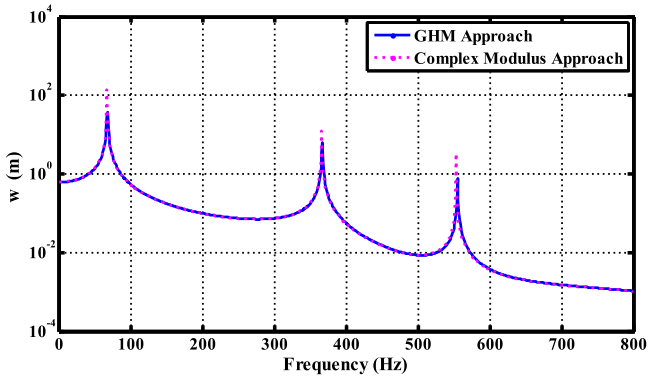

Figure 21. Linear frequency responses using the GHM and Complex modulus approach for a simply supported B/F/B-MEE plate.

are used as 1.822 × 106 Pa and 1140 kg m^{-3}, respectively [53]. To check the correctness of implementation of GHM method for modeling the viscoelastic materials, the linear frequency response for the transverse displacement of the multiferroic/MEE plate is computed separately using the conventional complex modulus approach and compared with the results of the GHM method. The First few modes of the plate at the point ($a/2$, $b/2$, $H/2$) are excited by applying a time harmonic load of 1 N. The frequency response functions obtained by the GHM method as well as by the standard complex modulus approach for a multiferroic composite plate with B/F/B stacking sequence has been illustrated in figure 21. It can be noticed from this figure that the frequency response curves obtained by both the methods are almost identical. As a result, the GHM method of modeling the viscoelastic material accurately estimates the damping characteristics plate. Figure 22 illustrates the comparison of linear frequency responses using the GHM method for a simply supported B/F/B plate. It can be observed from this figure that the considerable influence of viscoelastic materials on the frequency responses analogs to the piezoelectric layer of the plate. Further, viscoelastic layer increases the overall damping characteristics of the plate. As a result, control of transverse amplitude of the plate has been noticed.

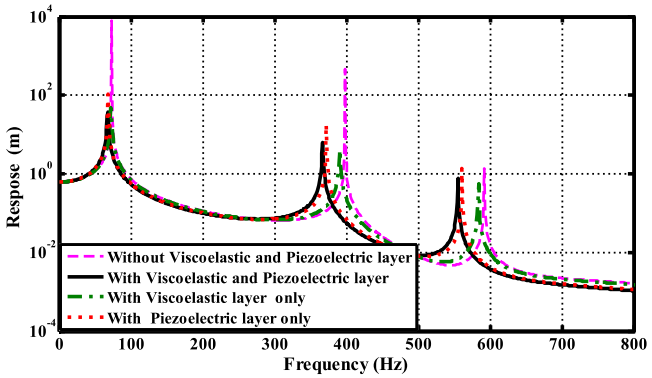

Figure 22. Comparison of linear frequency responses using the GHM method for a simply supported B/F/B MEE plate.

Table 6. Effect of coupled fields on the natural frequencies of the MEE plate.

	Mode	Uncoupled fields Frequency (ω)	Coupled fields Frequency (ω)
BFB	1	110	114
	2	358	366
FBF	1	108	112
	2	340	348

6. Conclusions

In this article, a layerwise shear deformation theory is used to analyze the smart damping of multiferroic composite plates. A finite element analysis of multiferroic/MEE plate attached with the patches of ACLD treatment has been carried out. The vertical actuation by the constraining layer of the patches is utilized for active damping of smart multiferroic composite plate. The best performance of the patches is achieved when the orientation angle (λ) of the fibers is 0° for both simply supported and clamped-clamped MEE plates. The electro-elastic and magneto-elastic couplings cause a marginal increase in stiffening of the multiferroic plates. These couplings improve the performance of the ACLD patches for attenuating the fundamental mode of vibration of the MEE plates. More importantly, the MEE plates integrated with the inactivated ACLD patches of negligible thickness (treating as without ACLD patches) have been analyzed by providing the control voltage directly across the thickness of the piezoelectric layers of the substrate plate. It is observed that even though the MEE plate is composed of smart piezoelectric/ferroelectric layers, the second mode of the MEE plate cannot be controlled by the activated piezoelectric layer with B/F/B stacking sequence. Further, the F/B/F plate does not show any response when activated by the piezoelectric layer. Also, the attenuation of the first mode of vibration is more in case of the ACLD of MEE plate than that in case of the control of the MEE plate by activating its piezoelectric layer. Based on the present study, it is suggested that the additional means for incorporating smartness in the flexible structure such as the ACLD patches are essentially required for the optimal control of the MEE plates while the required control voltage is very low.

Appendix

The various nodal vectors and shape functions appearing in equation (15) are

$$\{d_t^e\} = \left[\{d_{t1}^e\}^T \;\; \{d_{t2}^e\}^T \;\; \ldots \;\; \{d_{t8}^e\}^T\right]^T,$$
$$\{d_r^e\} = \left[\{d_{r1}^e\}^T \;\; \{d_{r2}^e\}^T \;\; \ldots \;\; \{d_{r8}^e\}^T\right]^T,$$

$$\{\phi^e\} = \left[\overline{\phi}_{11} \;\; \overline{\phi}_{21} \;\; \overline{\phi}_{12} \;\; \overline{\phi}_{22} \;\; \ldots \;\; \overline{\phi}_{18} \;\; \overline{\phi}_{28}\right]^T,$$
$$\{\overline{\psi}^e\} = \left[\overline{\psi}_1 \;\; \overline{\psi}_2 \;\; \ldots \;\; \overline{\psi}_8\right]^T,$$

$$[N_t] = [N_{t1} \;\; N_{t2} \;\; \ldots \;\; N_{t8}],$$
$$[N_r] = [N_{r1} \;\; N_{r2} \;\; \ldots \;\; N_{r8}],$$

$$[N_\phi] = \begin{bmatrix} n_1 & 0 & n_2 & 0 & \ldots & n_8 & 0 \\ 0 & n_1 & 0 & n_2 & \ldots & 0 & n_8 \end{bmatrix},$$

$$[N_\psi] = \left[N_{\psi 1} \;\; N_{\psi 2} \;\; \ldots \;\; N_{\psi 8}\right],$$
$$N_{ti} = n_i I_t,\; N_{ri} = n_i I_r.$$

where $[N_t]$, $[N_r]$, $[N_\phi]$ and $[N_\psi]$ are the (3 × 24), (8 × 64), (2 × 16) and (1 × 8) shape function matrices, respectively, I_t and I_r are the (3 × 3) and the (8 × 8) identity matrices.

ORCID iDs

S C Kattimani https://orcid.org/0000-0002-2477-3783

References

[1] Bailey T and Hubbard J E 1985 Distributed piezoelectric polymer active vibration control of a cantilever beam *J. Guid. Control Dyn.* **8** 605–11
[2] Crawley E F and Luis J D 1987 Use of piezoelectric actuators as elements of intelligent structures *AIAA J.* **25** 1371–85
[3] Baz A and Poh S 1988 Performance of an active control system with piezoelectric actuators *J. Sound Vib.* **126** 327–43
[4] Clark R L, Flemming M R and Fuller C R 1993 Piezoelectric actuators for distributed excitation of thin plates: a comparison between theory and experiment' *ASME J. Vib. Acoust.* **115** 332–9
[5] Reddy J N 1999 On laminate composite plates with integrated sensors and actuators *Eng. Struct.* **21** 568–93
[6] Baz A and Ro J 1996 Vibration control of plates with active constrained layer damping *Smart Mater. Struct.* **5** 272–80
[7] Park C H and Baz A 1999 Vibration control of bending modes of plates using active constrained layer damping *J. Sound Vib.* **227** 711–34
[8] Baz A 1998 Robust control of active constrained layer damping *J. Sound Vib.* **211** 467–80
[9] Dong S and Tong L 2001 Vibration control of plates using discretely distributed piezoelectric quasi-modal actuators/sensors *AIAA J.* **39** 1766–72
[10] Usik L and Joohong K 2001 Spectral element modelling for the beams treated with active constrained layer damping *Int. J. Solids Struct.* **38** 5679–702

[11] Azvine B, Tomlinson G R and Wynne R J 1995 Use of active constrained layer damping for controlling resonant *Smart Mater. Struct.* **4** 1–6

[12] Ray M C and Baz A 1997 Optimization of energy dissipation of active constrained layer damping treatments of plates *J. Sound Vib.* **208** 391–406

[13] Ray M C, Oh J and Baz A 2001 Active constrained layer damping of thin cylindrical shells *J. Sound Vib.* **240** 921–35

[14] Ray M C and Mallik N 2004 Active control of laminated composite beams using a piezoelectric fiber reinforced composite layer *Smart Mater. Struct.* **13** 146–52

[15] Ray M C and Reddy J N 2005 Active control of laminated cylindrical shells using piezoelectric fiber reinforced composites *Compos. Sci. Technol.* **65** 1226–36

[16] Ray M C and Pradhan A K 2006 Performance of vertically reinforced 1–3 piezoelectric composites for active damping of smart structures *Smart Mater. Struct.* **15** 631–41

[17] Ray M C and Pradhan A K 2007 On the use of vertically reinforced 1–3 piezoelectric composites for hybrid damping of laminated composite plates *Mech. Adv. Mater. Struct.* **14** 245–61

[18] Illaire H and Kropp W 2005 Quantification of damping mechanisms of active constrained layer treatments *J. Sound Vib.* **281** 189–217

[19] Kumar S R and Ray M C 2012 Active constrained layer damping of smart laminated composite sandwich plates using 1–3 piezoelectric composites' *Int. J. Mech. Mater. Des.* **8** 197–218

[20] Chantalakhana C and Stanway R 2001 Active constrained layer damping of clamped–clamped plate vibrations *J. Sound Vib.* **241** 755–77

[21] Araújo A L, Martins P, Mota Soares C M, Mota Soares C A and Herskovits J 2012 Damping optimization of hybrid active–passive sandwich composite structures *Adv. Eng. Softw.* **46** 69–74

[22] Araújo A L, Madeira J F A, Mota Soares C M and Mota Soares C A 2013 Optimal design for active damping in sandwich structures using the Direct MultiSearch method *Compos. Struct.* **105** 29–34

[23] Pan E and Heyliger P R 2002 Free vibrations of simply supported and multilayered magneto-electro-elastic plates *J. Sound Vib.* **252** 429–42

[24] Heyliger P R and Pan E 2004 Static fields inmagneto-electro-elastic laminates *AIAA J.* **42** 1435–43

[25] Liu M F and Chang T P 2010 Closed form expression for the vibration problem of a transversely isotropic magneto-electro-elastic plate *J. Appl. Mech.* **77** 1–8

[26] Ramirez F, Heyliger P R and Pan E 2006 Discrete layer solution to free vibrations of functionally graded magneto-electro-elastic plates *Mech. Adv. Mater. Struct.* **13** 249–66

[27] Buchanan G R 2004 Layered versus multiphase magneto-electro-elastic composites *Composites* B **35** 413–20

[28] Garcia Lage R, Mota Soares C M, Mota Soares C A and Reddy J N 2004 Layerwise partial mixed finite element analysis of magneto-electro-elastic plates *Comput. Struct.* **82** 1293–301

[29] Pan E 2001 Exact solution for simply supported and multilayered magneto-electro- elastic plates *ASME Trans.* **68** 608–18

[30] Pan E and Han F 2005 Exact solution for functionally graded and layered magneto-electro-elastic plates *Int. J. Eng. Sci.* **43** 321–39

[31] Wang J G, Chen L F and Fang S S 2003 State vector approach to analysis of multilayered magneto-electro-elastic plates *Int. J. Solids Struct.* **40** 1669–80

[32] Wang J, Lei Q and Feng Q 2010 State vector approach of free-vibration analysis of magneto-electro-elastic hybrid laminated plates *Compos. Struct.* **92** 1318–24

[33] Moita J M S, Mota Soares C M and Mota Soares C A 2009 Analysis of magneto-electro-elastic plates using higher order finite element model *Compos. Struct.* **91** 421–6

[34] Chen W Q, Lee K Y and Ding H J 2005 On free vibration of non-homogeneous transversely isotropic magneto-electro-elastic plates *J. Sound Vib.* **279** 237–51

[35] Bhangale R K and Ganesan N 2006 Free vibration of simply supported functionally graded and layered magneto-electro-elastic plates *J. Sound Vib.* **294** 1016–38

[36] Bhangale R K and Ganesan N 2005 Free vibration studies of simply supported non-homogeneous functionally graded magneto-electro-elastic finite cylindrical shells *J. Sound Vib.* **288** 412–22

[37] Chen J, Chen H and Pan E 2006 Free vibration of functionally graded, magneto-electro-elastic and multilayered plates *Acta Mech. Solida Sin.* **19** 160–6

[38] Guo J, Chen J and Pan E 2016 Static deformation of anisotropic layeredmagneto-electro-elastic plates based on modified couple-stress theory *Composites* B **107** 84–96

[39] Xin L and Hu Z 2015 Free vibration of simply supported and multilayered magneto-electro-elastic plates *Compos. Struct.* **121** 344–50

[40] Shooshtari A and Razavi S 2016 Vibration analysis of amagneto-electro-elastic rectangular plate based on a higher-order shear deformation theory *Latin Am. J. Solids Struct.* **13** 554–72

[41] Shooshtari A and Razavi S 2015a Nonlinear vibration analysis of rectangular magneto-electro-elastic thin plates *IJE Trans.* A **28** 136–44

[42] Shooshtari A and Razavi S 2015b Linear and nonlinear free vibration of multilayered magneto-electro-elastic doubly curved shells on elastic foundation *Composites* B **78** 95–108

[43] Razavi S and Shooshtari A 2015 Nonlinear free vibration of magneto-electro-elastic rectangular plates *Compos. Struct.* **119** 377–84

[44] Kattimani S C and Ray M C 2014 Smart damping of geometrically nonlinear vibrations of magneto-electro-elastic plates *Compos. Struct.* **114** 51–63

[45] Kattimani S C and Ray M C 2014 Active control of large amplitude vibrations of smart magneto-electro-elastic doubly curved shells *Int. J. Mech. Mater. Des.* **10** 351–78

[46] Kattimani S C and Ray M C 2015 Control of geometrically nonlinear vibrations of functionally graded Magneto-electro-elastic plates *Int. J. Mech. Sci.* **99** 154–67

[47] Kattimani S C 2015 *Active Control of Geometrically Nonlinear Vibrations of Magneto-electro-elastic Plates and Shells (IIT, Kharagpur, 2015-04)* http://idr.iitkgp.ac.in/xmlui/handle/123456789/5535

[48] Milazzo A 2014 Refined equivalent single layer formulations and finite elements for smart laminates free vibrations *Composites* B **61** 238–53

[49] Milazzo A 2014 Large deflection of magneto-electro-elastic laminated plates *Appl. Math. Modelling* **38** 1737–52

[50] Farajpour A, Hari Yzdi M R, Ratgoo A, Loghmani M and Mohammadi M 2016 Nonlocal nonlinear plate model for large amplitude vibration of magneto-electro-elastic nanoplates *Compos. Struct.* **140** 323–36

[51] Reddy J N 1996 *Mechanics of Laminated Composite Plates and Shells, Theory and Analysis* (Boca Raton, FL: CRC Press)

[52] Mc Tavish D J and Hughes P C 1993 Modelling of linear viscoelastic space structures *J. Vib. Acoust.* **115** 103–13

[53] Lim Y-H, Varadan V V and Varadan K V 2002 Closed loop finite element modeling of active constrained layer damping in the time domain analysis *Smart Mater. Struct.* **11** 89–97